Seasonal tidewater glacier terminus oscillations bias multi-decadal projections of ice mass change

Denis Felikson[1], Sophie Nowicki[2], Isabel J Nias[3], Mathieu Morlighem[4], and Helene Seroussi[5]

[1]NASA Goddard Space Flight Center
[2]University at Buffalo
[3]University of Liverpool
[4]University of California, Irvine
[5]Jet Propulsion Laboratory

November 22, 2022

Abstract

Numerical, process-based simulations of tidewater glacier evolution are necessary to project future sea-level change under various climate scenarios. Previous work has shown that nonlinearities in tidewater glacier and ice stream dynamics can lead to biases in simulated ice mass change in the presence of noisy forcings. Ice sheet modeling projections that will be used in the upcoming IPCC Assessment Report 6 (AR6) utilize atmospheric and oceanic forcings at annual temporal resolution, omitting any higher frequency forcings. Here, we quantify the effect of seasonal (<1 year) tidewater glacier terminus oscillations on decadal-scale (30 year) mass change. We use an idealized geometry to mimic realistic tidewater glacier geometries, and investigate the impact of the magnitude of seasonal oscillations, bed slope at the glacier terminus, and basal friction law. We find that omitting seasonal terminus motion results in biased mass change projections, with up to an 18% overestimate of mass loss when seasonality is neglected. The bias is most sensitive to the magnitude of the seasonal terminus oscillations and exhibits very little sensitivity to choice of friction law. Our results show that including seasonality is required to eliminate a potential bias in ice sheet mass change projections. In order to achieve this, seasonality in atmospheric and oceanic forcings must be adequately represented and observations of seasonal terminus positions and tidewater glacier thickness changes must be acquired to evaluate numerical models.

Seasonal tidewater glacier terminus oscillations bias multi-decadal projections of ice mass change

D. Felikson[1,2*], S. Nowicki[3], I. Nias[4], M. Morlighem[5], H. Seroussi[6]

[1]Cryospheric Sciences Laboratory, NASA Goddard Space Flight Center, Greenbelt, MD, USA
[2]Goddard Earth Sciences Technology and Research Studies and Investigations, Universities Space Research Association, Columbia, MD, USA
[3]Department of Geology, University at Buffalo, Buffalo, NY, USA
[4]School of Environmental Sciences, University of Liverpool, Liverpool, UK
[5]Department of Earth System Science, University of California, Irvine, Irvine, CA, USA
[6]Jet Propulsion Laboratory, California Institute of Technology, Pasadena, CA, USA

Key Points:

- Seasonal terminus oscillations induce a systematic decrease in multi-decadal mass loss of retreating glaciers
- Mass loss bias increases with magnitude of oscillations in ice front position
- Mass loss bias is more sensitive to bed slope at the terminus than to sliding law

*Address

Corresponding author: Denis Felikson, `denis.felikson@nasa.gov`

Abstract

Numerical, process-based simulations of tidewater glacier evolution are necessary to project future sea-level change under various climate scenarios. Previous work has shown that nonlinearities in tidewater glacier and ice stream dynamics can lead to biases in simulated ice mass change in the presence of noisy forcings. Ice sheet modeling projections that will be used in the upcoming IPCC Assessment Report 6 (AR6) utilize atmospheric and oceanic forcings at annual temporal resolution, omitting any higher frequency forcings. Here, we quantify the effect of seasonal (<1 year) tidewater glacier terminus oscillations on decadal-scale (30 year) mass change. We use an idealized geometry to mimic realistic tidewater glacier geometries, and investigate the impact of the magnitude of seasonal oscillations, bed slope at the glacier terminus, and basal friction law. We find that omitting seasonal terminus motion results in biased mass change projections, with up to an 18% overestimate of mass loss when seasonality is neglected. The bias is most sensitive to the magnitude of the seasonal terminus oscillations and exhibits very little sensitivity to choice of friction law. Our results show that including seasonality is required to eliminate a potential bias in ice sheet mass change projections. In order to achieve this, seasonality in atmospheric and oceanic forcings must be adequately represented and observations of seasonal terminus positions and tidewater glacier thickness changes must be acquired to evaluate numerical models.

Plain Language Summary

Computer models are required to predict how glaciers will evolve under future climate warming. Past studies have shown that rapid changes in external variables that affect glaciers can lead to a permanent shift in their state. However, not all computer models take these rapid changes into account. For example, model predictions of the ice sheets that will be used in the upcoming IPCC Assessment Report 6 (AR6) leave out seasonal changes of glaciers. In this paper, we set up a computer model to resemble a typical glacier and we run the model by forcing the glacier to retreat either with or without seasonal terminus movement. Our results reveal that leaving out seasonality causes up to an 18% overestimate of mass loss. We repeat these runs with varying amounts of retreat, different friction laws, and variable slope of the bed underneath the glacier terminus. We find that the overestimate is most sensitive to the amount of seasonal advance and retreat and least sensitive to the friction law. Our results show that computer models must take the seasonal changes into account in order to make accurate predictions and to avoid overestimating mass loss of glaciers in the future.

1 Introduction

Marine-terminating ice constitutes over one third of Earth's glaciated regions by area (Gardner et al., 2013) and has been responsible for >40% of mass loss in Greenland (Mouginot et al., 2019) and >75% of mass loss in Antarctica (Rignot et al., 2019) over the last 20 years. Discharge of ice from tidewater outlet glaciers that drain the Greenland Ice Sheet (GrIS) is projected to be responsible for 50±20% of GrIS mass loss by 2100 (Choi et al., 2021). Observations have shown that rapid retreat of GrIS outlet glaciers initiated in the mid-1990s or earlier (Fahrner et al., 2021), with synchronous retreat initiation for individual glaciers within particular regions (Catania et al., 2018), and that nearly all glaciers around the GrIS experienced retreat from 2000 to 2010 (Murray et al., 2015). Terminus retreat has been identified as the primary driver of outlet glacier acceleration at particular glaciers (e.g., Bondzio et al., 2017; Muresan et al., 2016). Numerical ice sheet models are being used to simulate ice sheet dynamic response to future climate projections and provide sea-level rise estimates via efforts such as the Ice Sheet Modeling Intercomparison for the Coupled Model Intercomparison Project Phase 6 (ISMIP6; Nowicki et al., 2020; Goelzer et al., 2020;

Seroussi et al., 2020). Some of these continental-scale models are now being run at high enough spatial resolution to resolve dynamic changes of outlet glaciers at the ice sheet margin. However, to keep computational and implementation expense low and to allow for broad participation of ice sheet models in ISMIP6, ocean and atmosphere forcings were specified at an annual frequency and, thus, models did not simulate ice sheet response to seasonal forcing (Nowicki et al., 2020).

Past numerical modeling studies have shown that high-frequency forcing can bias glacier and ice stream response. Changes in the magnitude of natural random variability in the length of an ice shelf can cause changes in the mean location of the grounding line of a glacier (Robel et al., 2018). Modeling of Thwaites Glacier, West Antarctica, showed that, when submarine ice shelf melt is modeled using a varying ocean temperature profile or stochastic ocean-induced melt, it can cause a delay in simulated grounding line retreat and mass loss (Hoffman et al., 2019; Robel et al., 2019). Climate variability can also give rise to equilibrium states in ice streams not attainable in the absence of stochastic forcing (Mantelli et al., 2016).

Tidewater glacier termini rest on both prograde and retrograde bed topography and exhibit a variety of magnitudes of seasonal oscillations. To our knowledge, no systematic study of seasonal terminus motion for a representative sample of all tidewater glaciers has been done. However, there have been studies focusing on individual glaciers or groups of outlet glaciers around the GrIS that have revealed a variety of seasonal terminus oscillation magnitudes. Bevan et al. (2012) compiled a 25-year record of terminus position changes of 16 of Greenland's major outlet glaciers showing seasonal oscillations that varied in amplitude among the glaciers with several glaciers exhibiting oscillations larger than 2 km in amplitude (Helheim, Kangerdlugssuaq, Jakobshavn, Rink). Schild and Hamilton (2013) quantified seasonal retreat for five of Greenland's largest outlets (Daugaard Jensen, Kangerdlugssuaq and Helheim glaciers in East Greenland, and Jakobshavn Isbræ and Rink Isbræ in West Greenland) between 2001 and 2010 and found the glaciers' average seasonal retreat to be between 960 and 5540 m. Moon et al. (2015) found that the mean annual range in terminus position varied from 150 to 1,250 m across 16 glaciers in Northwest Greenland. Fried et al. (2018) found up to 1,500 m of seasonal terminus oscillations for glaciers in West Greenland, although there was notable variability from glacier to glacier, with some glaciers retreating as little as 50 m during particular years, as well as heterogeneity in terminus position across individual glacier widths within a given season.

Additionally, 100-year simulations of tidewater glaciers and ice streams are sensitive to the form and parameters of the basal friction parameterization, typically called the "sliding law". This parameterization describes the relationship between basal shear stress and sliding velocity and both the structure and parameters of the sliding law remain an active area of research: several sliding laws have been proposed and are in use by numerical ice flow models (Budd et al., 1979; Weertman, 1957; Schoof, 2005; Gagliardini et al., 2007; Tsai et al., 2015) but few direct observations exist to validate them. Projections of the Antarctic Ice Sheet (AIS) found that the contribution of the AIS to global sea level increases with increasing sliding exponent, using the Weertman sliding law (Bulthuis et al., 2019; Ritz et al., 2015; Sun et al., 2020). The form of the sliding law affects the sensitivity of numerical ice flow models to changes in mesh resolution and to sub-element melt parameterizations in terms of both grounding line retreat and ice volume loss (Seroussi & Morlighem, 2018). Idealized geometry simulations show that relative volume loss can range from 0 to 15%, depending on the form of the sliding law, even when the conversion between laws is perfect and the initial basal stress is identical (Brondex et al., 2017). Simulations of the ice streams in the Amundsen Sea Embayment, Antarctica, have also been shown to be highly sensitive to sliding law formulation, with higher sensitivity to sliding laws that include a dependence on effective pressure at the ice-bed interface (Brondex et al., 2019). There is also an interplay between sliding law parameterizations and uncertainty in bed topography, with linear sliding laws causing a smaller shift in mass loss than non-linear sliding laws when uncertainty in bed topography is sampled (Nias et al., 2016).

Here, we use a numerical model to simulate the ice flow of an idealized tidewater glacier and to quantify the effect of seasonal terminus oscillations on its projected decadal-scale mass change. Starting from a steady-state configuration, we perform two simulations. In the first one, the glacier terminus retreats from its initial position by a specified distance. In the second one, oscillations with a one-year period are added to the overall terminus retreat of the first case. We perform these two simulations using three magnitudes of specified retreat, two commonly used sliding laws, and for glacier terminus located on either prograde or retrograde bed slope. In our simulations, we specify the terminus position at any given time during the simulations and, thus, we do not explore the effect of calving laws. Our goal is to understand the impact of seasonal terminus oscillations on centennial ice sheet mass change projections, such as those created for ISMIP6 (Nowicki et al., 2020). Thus, we set up our numerical model simulations with common parameterizations used in ISMIP6 and mesh resolution that typically represents the finest scale used for continental-scale models of the Greenland Ice Sheet (Goelzer et al., 2020).

We first describe our numerical model setup in Section 2.1, including a description of the geometry, boundary conditions, and model parameterizations. We then describe how the numerical model is initialized in Section 2.2 and the forward model simulations in Section 2.3. We present the thickness and velocity changes caused by seasonal terminus oscillations and compare mass change of glaciers with and without oscillations in Section 3. We discuss the broader implications of our idealized model simulations and we suggest future research directions in Section 4.

2 Methods

2.1 Model setup

We perform numerical simulations using the Ice-sheet and Sea-level System Model (ISSM; Larour et al., 2012). We use the 2-dimensional shelfy-stream approximation (SSA; MacAyeal, 1989), a stress-balance approximation appropriate for fast-flowing tidewater glaciers. Terminus position is specified using the level-set method (Bondzio et al., 2016). The level set is a real-valued, differentiable function with values defined at each model node, and the glacier terminus is defined to be the zero-level contour of the level set. This contour can bisect model elements, continuously tracking the position of the zero-level contour, even though the model considers elements to be either entirely filled with ice or not filled with ice.

The bed geometry that we use is adapted from the Marine Ice Sheet Ocean Model Intercomparison Project (MISOMIP; Asay-Davis et al., 2016; Cornford et al., 2020). We modify the MISOMIP geometry to be more representative of tidewater glacier beds by steepening the sidewalls, narrowing the fjord, shortening the domain to focus on the near-terminus region, and removing all floating ice. We follow the notation of Asay-Davis et al. (2016) to specify bedrock topography, shown in Fig. 1, as:

$$B_x\left(x\right) = B_0 + B_2\tilde{x}^2 + B_4\tilde{x}^4 + B_6\tilde{x}^6 \tag{1}$$

$$\tilde{x} = x/\bar{x} \tag{2}$$

$$B_y\left(y\right) = \frac{d_c}{1 + e^{-2/f_c\times(y-L_y/2-w_c)}} + \frac{d_c}{1 + e^{-2/f_c\times(y-L_y/2+w_c)}} \tag{3}$$

$$z_B(x,y) = B_x(x) + B_y(y) \tag{4}$$

with parameter values defined in Table 1.

Table 1. Parameters for the model geometry and boundary conditions.

Parameter	Value	Description
L_x	30 km	Domain length (along ice flow)
L_y	8 km	Domain width (across ice flow)
B_0	150 m	Bedrock topography at $x = 0$
B_2	-728.8 m	Second bedrock topography coefficient
B_4	150 m	Third bedrock topography coefficient
B_6	150 m	Fourth bedrock topography coefficient
$\bar{x}$	15000 m	Characteristic along-flow length scale of the bedrock
f_c	400 m	Characteristic width of the side walls of the channel
d_c	1000 m	Depth of the trough compared with the side walls
w_c	2800 m	Half-width of the trough

Another difference between our model setup and that of MISOMIP is that we specify ice flow into our domain at the in-flow boundary (x=0 km) using the following relationship, an arbitrary analytical expression designed to be similar to the expression for bed topography:

$$v_x(y) = 690 - \frac{700}{1 + e^{(2/f_c)(y - L_y/2 + w_c)}} - \frac{700}{1 + e^{(-2/f_c)(y - L_y/2 - w_c)}} \quad \text{m/a} \tag{5}$$

The surface elevation at the in-flow boundary is constrained to be 4 km. At the southern (y=0 km) and northern (y=8 km) boundaries, ice is allowed to freely slip in the x-direction (along flow) but constrained to have $v_y = 0$, meaning that ice cannot flow into or out of the model domain along these boundaries. A Neumann boundary condition accounting for water pressure is applied at elements along the ice front.

To simulate a typical surface mass balance (SMB) for a tidewater glacier, we use the following relationship:

$$\text{SMB}(x) = -\frac{0.5}{30000}x \quad \text{m/a ice eq.} \tag{6}$$

At the western boundary (the in-flow boundary of the model domain) SMB is therefore 0 m/yr, and at the eastern boundary, SMB is -0.5 m/yr.

In the experiments, we compare the glacier's response using two commonly-used basal friction laws. The first is a power law that includes effective pressure (Budd et al., 1979), assumed here to be equal to the pressure of the ice above hydrostatic equilibrium:

$$\tau_b = C_B u_B^m N^q \tag{7}$$

The second is a law that describes ice sliding over a hard bed and neglects effective pressure (Weertman, 1957):

$$\tau_b = C_W u_B^m \tag{8}$$

We consider the case of linear sliding ($m = 1$) and specify the coefficients C_B and C_W such that the initial basal stress is identical for both friction laws (Section 2.2).

Ice rheology is spatially uniform and follows Glen's flow law with flow exponent $n = 3$ and rate factor $A = 1.4 \times 10^{-24}$ s^{-1} Pa^{-3}, corresponding to an ice temperature of approximately -3°C.

We generate a mesh using the Bidimensional Anisotropic Mesh Generator (BAMG) package, developed by Hecht (2006), with maximum edge length specified to be 200 m. The resulting mesh has 13,264 triangular elements and 6,823 vertices over the model domain.

2.2 Model initialization

To initialize the simulations, we spin up the model until it has reached a steady state, at which point the change in mass is <0.001 Gt/yr. We initialize two glacier geometries: one with the terminus at x = 24 km, on a retrograde bed slope, and the other with the terminus at x = 26 km, on a prograde bed slope (Fig. 1). The initial steady-state glacier geometries are obtained using the Budd sliding law (Eqn. 7) with the friction coefficient specified as:

$$C_B = \frac{180}{1 + e^{(-2/f_c)(y - L_y/2 - w_c)}} + \frac{180}{1 + e^{(2/f_c)(y - L_y/2 - w_c)}} \tag{9}$$

We then solve for C_W by equating basal shear stress, τ_b, for the two friction laws, keeping velocity, u, constant. To check our conversion between friction coefficients, we solve the stress balance equations with each of the two sliding laws and corresponding friction coefficients to obtain ice velocity. For both initializations, the stress balance solutions result in mean relative differences in velocity <0.001 m/yr, indicating that the stress balances, after converting from the Budd sliding law to the Weertman sliding law, are nearly identical.

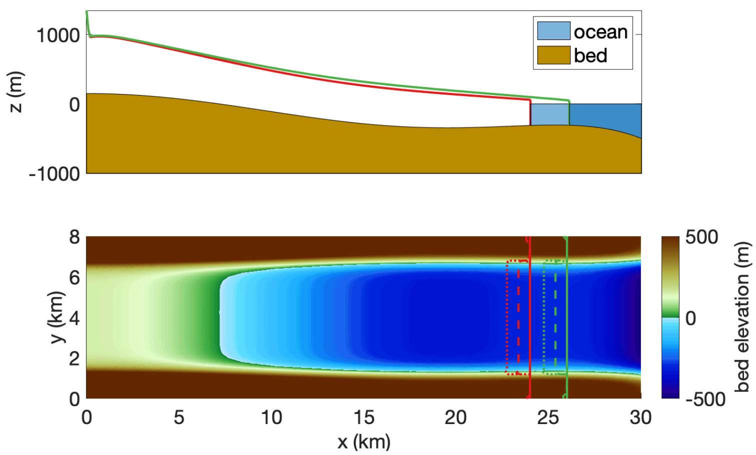

Figure 1. (a) Initial glacier profiles for terminus position on retrograde bed slope (x = 24 km, red line) and on prograde bed slope (x = 26 km, green line). Ice flows from left to right, with the glacier surfaces and termini shown in green (prograde bed slope) and red (retrograde bed slope). (b) Terminus positions in glacier model simulations for glaciers with terminus on retrograde bed slope (red) and on prograde bed slope (green), shown on top of bed topography. In the seasonality simulations, termini oscillate between the advanced (solid) and retreated (dotted) positions. In the no-seasonality simulations, the termini retreat to the mean position (dashed) and remain stationary there.

2.3 Experiments

Our transient experiments test an idealized glacier's response to oscillations in terminus position, with all other forcings remaining constant. We run 30-year transient simulations, prescribing retreat and advance of the terminus with an annual period and various magnitudes. Fig. 1 shows the initial glacier geometry, including initial terminus positions (solid lines) and the amplitude of the seasonal retreats (dotted lines). We have designed our simulations such that, when the terminus position advances, it does not exceed the ice speed at the front. In the transient experiments, the terminus oscillates between the solid lines and dotted lines with a period of one year. We compare mass change for the simulation with terminus oscillations against a "no seasonality" simulation in which the terminus retreats to a position that represents the average position of the experiment with seasonality (dashed lines in Fig. 1b). Terminus position is prescribed using time-varying level sets and ISSM linearly interpolates the level set through time at each model step, which is set to 0.01 years.

The two simulations (with and without seasonality) are repeated for different model parameters to test the effect of the basal sliding law, bed slope at the terminus, and magnitude of seasonal oscillations. We run the simulations for each combination of two initial terminus positions (x=24 km and x=26 km), two sliding laws (Weertman and Budd), and three magnitudes of seasonal terminus oscillations (625 m, 937.5 m, and 1250 m). For each of the 12 combinations of parameters, we compare the time series of mass change for the simulation with seasonality (ΔM_s) against the simulation with no seasonality (ΔM_n). For the simulations with 1250-m terminus oscillations, two additional simulations are performed for each combination, one in which the terminus position remains fixed at its most advanced position and another in which the terminus retreats to and remains fixed at its most retreated seasonal position.

3 Results

Over the course of the simulation, the glacier with seasonal terminus oscillations goes through cycles of retreat/advance, acceleration/deceleration, and thinning/thickening. We present these results solely to illustrate the cycle that the glacier undergoes over the first year of the simulation, when the glacier is starting to adjust to it's new dynamic regime, and the last year of the simulation, once the cycle has stabilized. Figure 2 shows thickness and velocity changes (Δh_s and Δv_s) at quarter-year increments during the first and last simulation years. In year 1, the glacier thins and accelerates over the first half of the year in response to terminus retreat (Figs. 2 a-b and e-f), with >1.5 m of thinning and >150 m/yr of acceleration extending over 12 km along the glacier centerline from the original terminus (x=24 km) at year 0.50. During the second half of the year, in response to terminus re-advance, the glacier thickens and decelerates (Figs. 2 i-j and m-n), with >1.5 m of thickening and >150 m/yr of deceleration extending over 6 km along the glacier centerline from the original terminus (x=24 km) at year 1.00. In the final year of the simulation, the glacier goes through a similar seasonal cycle but the spatial pattern differs from the first year of the simulation. During the first quarter of the final year, the glacier is still thickening in response to the advance from the previous year (Fig. 2c), although acceleration has begun in response to retreat (Fig. 2d). Halfway through the final year, >1.5 m of thinning extends over 7.5 km (Fig. 2g) and >150 m/yr of acceleration extends over 11.5 km from the original terminus along the glacier centerline (Fig. 2h). During the second half of the year, the glacier thickens and decelerates (Fig. 2 k-l and o-p), with >1.5 m of thickening extending over 7.5 km and deceleration extending over 8.5 km from the original terminus along the glacier centerline. The cycle of the final simulation year will repeat into the future in the absence of any additional changes in the forcings.

At the end of the 30-year simulation, the oscillating glacier is, on average, thicker and slower than the non-oscillating glacier. Figure 3 shows the thickness and velocity differences between the oscillating and non-oscillating glaciers at selected times during the final year of the simulation. Throughout this final year, the non-oscillating glacier has reached a new steady state and its thickness and velocity are nearly constant throughout the year. As the oscillating glacier begins its retreat in year 29.25, the oscillating glacier is thicker and slower than the non-oscillating glacier (Figs. 3a-b), following from the re-advance of the previous year. At its most retreated in year 29.50, the oscillating glacier accelerates to a speed that is faster than the non-oscillating

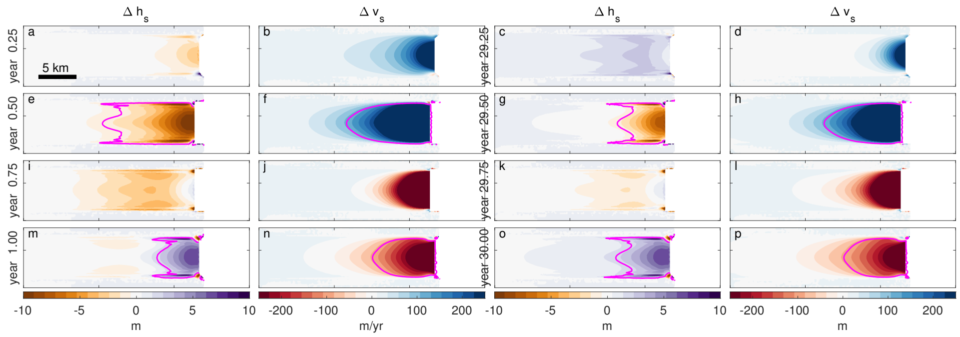

Figure 2. Glacier thickness and velocity change in response to oscillating glacier terminus during the first and last simulation years. This figure shows the simulation with terminus on retrograde bed slope (initial position at x=24 km), Budd sliding, and 1250-m magnitude of oscillations. Each row shows change in variables in map view at 0.25-yr increments. The first and second columns show thickness and velocity change from year 1; the third and fourth columns show thickness and velocity change from year 30. Magenta contours show extent of >1.5 m of thinning (e and g) and thickening (m and o) and >150 m/yr of acceleration (f and h) and deceleration (n and p).

glacier (Fig. 3d) and begins to thin (Fig. 3c). During re-advance, the thinning that was initiated by terminus retreat has spread upstream but, even at its thinnest state during this year, the oscillating glacier remains thicker than the non-oscillating glacier except for a small patch within ∼2 km of the terminus (Fig. 3e). At this stage, the oscillating glacier decelerates to a speed that is slower than the non-oscillating glacier (Fig. 3f) and continues to decelerate as the re-advance completes (Fig. 3h). On average over the course of this year, the oscillating glacier is thicker (Fig. 3i) and slower (Fig. 3j) than the non-oscillating glacier across the entire glacier domain. The largest thickness anomaly is mostly stored between 5 and 15 km upstream of the terminus. Further upstream, the thickness of the oscillating glacier tapers down to that of the stationary glacier. Closer to the terminus, the thickness anomaly tapers off, as well, as this is the region that thins due to seasonal retreat.

Because the oscillating glacier is thicker than the non-oscillating glacier, it has retained more of its mass than the non-oscillating glacier following retreat from its initial terminus position. In other words, the oscillating glacier experiences less mass loss than the non-oscillating glacier. Time series of change in glacier mass above floatation show that the annual mean mass changes for the simulation including seasonal terminus oscillations are 17.5% and 17.9% less than the simulations without oscillations for the Budd and Weertman sliding laws on retrograde bed slopes with 1250-m magnitude oscillations, respectively (Fig. 4, Table 2). On prograde bed slope, terminus oscillations result in less mass loss than non-oscillating glacier and with slightly lower offset (13.9% and 14.6% for the two sliding laws, Table 2). Offsets in mass loss increase with increasing magnitude of oscillations for both sliding laws. For the smallest magnitude of terminus oscillations (625 m), the glaciers with termini on retrograde bed slope lose more mass in simulations with terminus oscillations, although the offsets are <2%. For 937.5-m oscillations, the offsets increase to 9% for Weertman sliding and 14% for Budd sliding. For 1250-m oscillations, the offsets increase further to 13% for Weertman sliding and 18% for Budd sliding, respectively (Table 2). To bound our results, we run additional simulations in which the terminus stays fixed at its original position and in which the terminus retreats to the most retreated seasonal position and remains fixed there (Fig. S1). With terminus retreat to the most retreated seasonal positions,

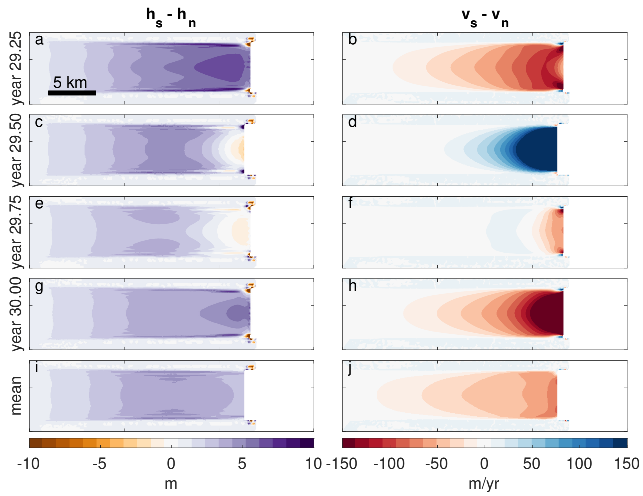

Figure 3. Differences in glacier thickness and velocity between oscillating and non-oscillating glaciers during year 30 of the simulation. This figure compares the simulation with terminus on retrograde bed slope (initial position at x=24 km), Budd sliding, and 1250-m magnitude of oscillations against the simulation with the same parameters but without oscillations (terminus retreats to the average position of the oscillating glacier). Each row shows variables in map view at 0.25-yr increments, with the last row showing the annual mean. The first column shows differences in thickness ($h_s - h_n$) and the second column shows differences in velocity ($v_s - v_n$).

the simulations result in approximately twice the mass loss as the simulations with terminus retreat to the average of the oscillating positions. For Weertman sliding, the simulations result in 1.24 and 1.27 Gt of mass loss on prograde and retrograde bed slopes, respectively, and the simulations with Budd sliding result in 3.34 and 3.46 Gt of mass loss on prograde and retrograde bed slopes, respectively.

Mass loss offsets are more sensitive to bed slope at the terminus than to the choice of sliding law. With 1250-m oscillations, both sliding laws cause 17.5-17.9% offset on retrograde bed slope (light blue and red circles on Fig. 5b) and 13.9-14.6% offset on a prograde bed slope (dark blue and red circles on Fig. 5b). The sliding law has an effect on overall mass loss, regardless of whether or not terminus oscillations are simulated. For both retrograde and prograde bed slopes, Budd sliding results in more mass loss than Weertman by a factor of between 2.7 and 2.8.

4 Discussion

Our results show that omitting seasonal terminus oscillations from simulations of tidewater glacier retreat can lead to a bias in centennial projections of ice sheet mass loss. Glaciers with small seasonal oscillations (625 m) exhibit little bias (<2%), regardless of sliding law or bed slope. On the other hand, glaciers with large seasonal oscillations (1250 m) exhibit large bias, up to 18%. Thus, for glaciers with large seasonal terminus oscillations, mass loss is overestimated when terminus seasonality is omitted from simulations. The seasonal oscillation magnitudes in our experiments serve as end members because typical observed seasonal terminus oscillations do not exceed 1500 m whereas oscillations of 625 m yield almost no discrepancy in mass change when compared to simulations without seasonal oscillations. Our results suggest that ice-sheet-wide projections of mass loss that omit seasonal forcing therefore overestimate ice sheet contribution to sea level rise. For example, the Greenland projection

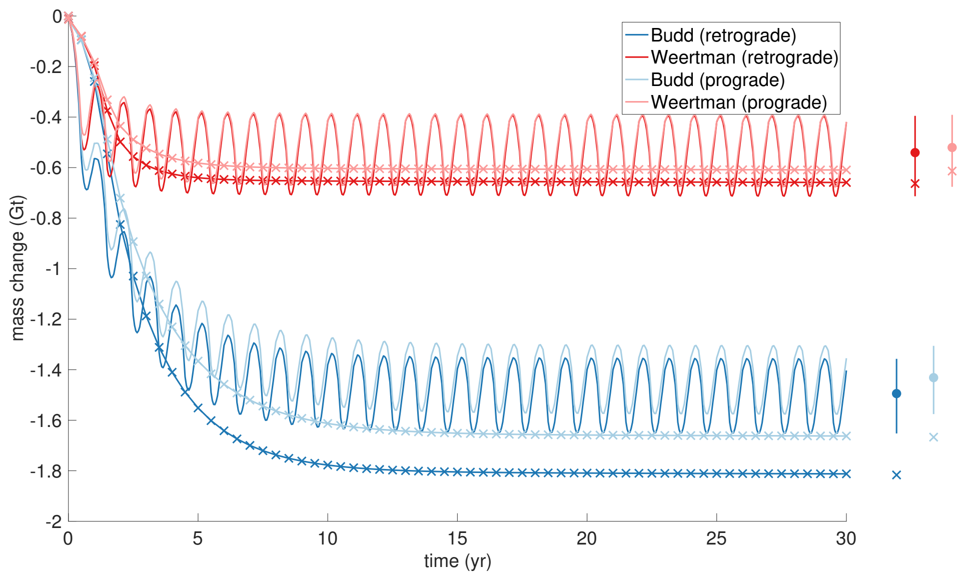

Figure 4. Glacier mass change for Budd (blue) and Weertman (red) sliding laws on prograde (lighter lines) and retrograde (darker lines) bed slope. Change in mass above floatation shown for two simulations: no seasonality (line with x's) and with seasonality (no x's). To the right of the time series, filled circles represent mean mass change and vertical lines represent seasonal amplitude of mass change during final year of simulation.

Table 2. Mass change for model simulations, calculated as the difference between annual-mean glacier mass over the last year of each simulation and initial glacier mass. Percent differences ("% diff" column) are calculated with respect to the no seasonality mass change, with positive (negative) values indicating more (less) mass loss than the no-seasonality simulation.

sliding law	bed slope at terminus	magnitude	ΔM_n	ΔM_s	% diff
Budd	retrograde	625	-0.78	-0.79	+1.8
		937.5	-1.30	-1.16	-11.1
		1250	-1.81	-1.49	-17.5
	prograde	625	-0.79	-0.78	-0.4
		937.5	-1.23	-1.11	-9.2
		1250	-1.66	-1.43	-13.9
Weertman	retrograde	625	-0.29	-0.29	+0.2
		937.5	-0.48	-0.42	-12.2
		1250	-0.66	-0.54	-17.9
	prograde	625	-0.29	-0.29	-1.5
		937.5	-0.45	-0.41	-9.6
		1250	-0.61	-0.52	-14.6

simulations produced for ISMIP6 (Goelzer et al., 2020) use forcings specified at annual intervals (Nowicki et al., 2020). Thus, ISMIP6 projections do not include seasonal tidewater glacier terminus oscillations and the resulting mass change projections may be biased. Future ice sheet modeling projects should include seasonality in tidewater glacier terminus forcing in order to achieve unbiased multi-decadal projections.

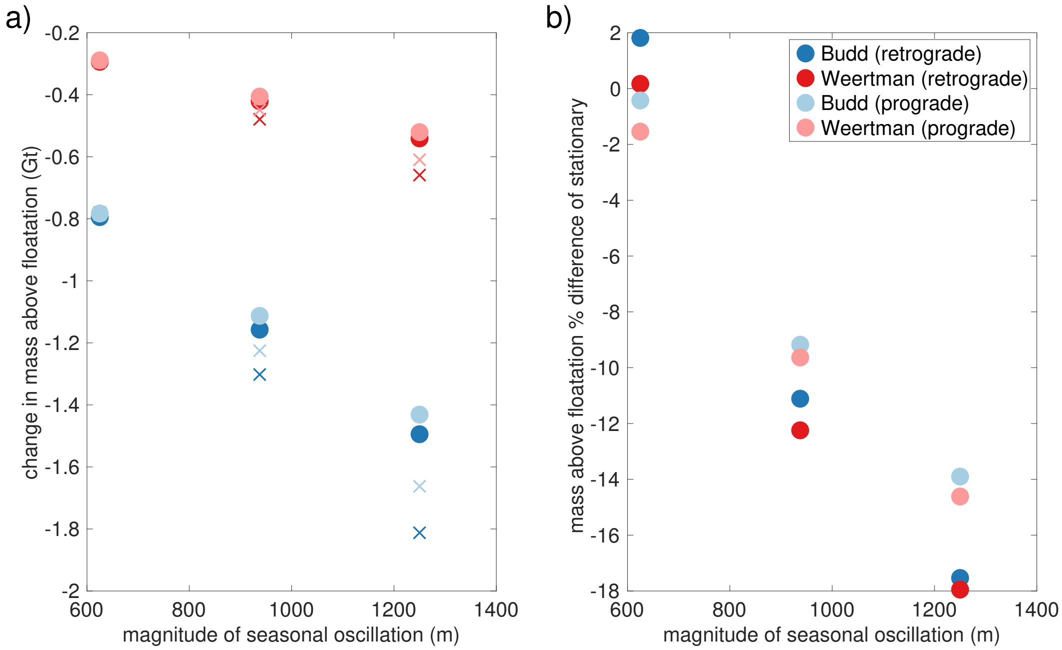

Figure 5. Glacier mass change for all simulations. (**a**) Change in mass above floatation for simulations with oscillating terminus (filled circles) and without oscillations (x's). (**b**) Percent difference in mass loss between simulation with and without seasonal terminus oscillations.

In our experiments, all simulated glacier mass change is caused solely by perturbations in terminus position. All other forcings are kept constant throughout the model runs. In other numerical modeling experiments, as well as in the real world, other forcings can initiate seasonal variability in tidewater glacier mass change, including changes in basal sliding due to summer runoff (Smith et al., 2021; Davison et al., 2020; Vijay et al., 2019; Moon et al., 2014) and cryo-hydrologic warming (Phillips et al., 2010). Further work is needed to quantify the potential impact of these forcings on our results.

Omitting terminus seasonality has additional implications for calibration of numerical ice sheet models. Previous studies that have performed transient calibration of models use discrepancies between observed and modeled mass and surface elevation change to evaluate models (Ritz et al., 2015; Ruckert et al., 2017; Nias et al., 2019; Edwards et al., 2019). Our results show that models that do not include seasonality result in biased mass change and, thus, calibrating models without seasonality using observations, which do inherently include the response to seasonality in terminus forcing, can result in biases in calibrated model parameters and projections.

The bias in modeled mass loss that we have quantified is more sensitive to bed topography than to the chosen sliding law (Fig. 5). As the magnitude of terminus oscillations increases, the discrepancy in mass loss between simulations with and without oscillations increases from between -1.5 and +1.8% for the smallest 625-m oscillations to between -14.6 and -17.9% for the largest 1250-m oscillations. At any given oscillation magnitude, the range in discrepancies is <1.6% for the different sliding laws and up to 3.6% for different bed slopes. Thus, bed slope at the terminus has more effect on the discrepancy, with the largest discrepancies occurring when the terminus oscillates on retrograde bed slope.

We find that simulations with Budd sliding result in more mass loss than simulations with Weertman sliding by a factor of 2.7-2.8. In model simulations of the Amundsen Sea Embayment (ASE), Antarctica, Brondex et al. (2019) found $\sim$5 times more loss in volume above floatation for simulations using Budd sliding versus Weertman sliding. Their numerical model allowed the grounding line to evolve, with Budd sliding resulting in more grounding line retreat than Weertman sliding. Thus, in the simulations of Brondex et al. (2019), the sliding law could affect the grounded ice via changes in basal shear stress and via reduced basal drag through a reduction in grounded area. This establishes a positive feedback because, as the grounding line retreats, the grounded ice thins, bringing more ice to floatation and causing the grounding line to retreat further. By contrast, in our simulations, the grounding line position was specified using the levelset method and, by design, we set it to be identical in experiments for both sliding laws. Thus, in our simulations, the sliding law can affect mass change via changes in basal shear stress but not via changes in grounding line position. Adding this potential feedback in the simulations could further amplify the differences between Budd and Weertman sliding in our tidewater glacier simulations.

To better understand the effect of neglecting terminus oscillations on projection bias, similar simulations need to be performed using real tidewater glacier geometries. To provide a controlled experiment with easily interpretable results, we used bed geometry and model parameters that are specified by smooth analytical functions that are constant in time. Our simulations were performed for one specified bed topography to focus on the impact of sliding law and magnitude of oscillations. For real glaciers, we anticipate heterogeneity in along- and across-flow bed roughness and basal traction to affect the discrepancy in mass change between simulations with an oscillating terminus and ones without oscillations. There will also be a variety of trough widths, bed depth, and sill heights for real glaciers. Thus, it is necessary to perform similar experiments using simulations initialized to represent real tidewater glaciers. Experiments on real glaciers will also help to reveal the glaciers for which including seasonal terminus forcing is critical and those for which seasonality can be omitted.

Improved observations at seasonal temporal resolution are required to properly simulate and measure seasonal ice sheet dynamic processes. Recent advances in automatic detection methods for measuring terminus positions, previously a labor-intensive manual process, have started to produce dense time series of terminus positions for glaciers around the ice sheets (Cheng et al., 2021; Zhang et al., 2019). These datasets are critical for producing ice sheet hindcasts and understanding the processes that control terminus positions on seasonal timescales. Global observations of ice velocity at 120-m spatial resolution have recently been compiled at monthly temporal resolution (Gardner et al., 2019, 2018). Ice mass change observations from satellite gravimetry, also at monthly temporal resolution, have been available since the early 2000s (Jacob et al., 2012; Schrama & Wouters, 2011; Luthcke et al., 2013; Velicogna & Wahr, 2013; The IMBIE team, 2018; Shepherd et al., 2020; Velicogna et al., 2020). Satellite gravimetry measurements produce mass change estimates on scales of hundreds of kilometers and ice sheet surface elevation change measurements from altimetry or photogrammetry are required to localize changes to the scale of individual tidewater glaciers (Howat et al., 2008; Felikson et al., 2017). Until the recent launch of ICESat-2, these altimetry measurements were too coarse in time to provide thickness changes of most tidewater glaciers on a seasonal timescale (Csatho et al., 2014). ICESat-2 will provide measurements of the ice surface over the ice sheets at a 91-day repeat cycle, allowing seasonal thickness changes of tidewater outlet glaciers to be estimated. However, over tidewater glaciers outside of the ice sheets, ICESat-2 has not collected repeating measurements and other methods, such as photogrammetry or airborne altimetry, must be used to obtain seasonal thickness change. To enable comparison of models to observations, datasets of surface elevation change at seasonal resolution must be produced at the spatial scales of tidewater glaciers.

In addition to observations, atmospheric and oceanic forcings must also adequately represent seasonal variations, both in the past and for future projections. Recent work by Barthel et al. (2020) evaluated global climate models from the Coupled Model Intercomparison Project Phase 5 (CMIP5) on their ability to reproduce the observed polar climate over 1980 to 2004. Modeled summer and winter air temperatures over both ice sheets were compared against reanalysis data products, thereby evaluating each model's ability to reproduce the amplitude of the seasonal cycle of air temperature. For other variables, including ocean temperature, annual means were used as a basis of comparison and, thus, the seasonal amplitudes of ocean temperatures were not evaluated due to the lack of observations. To improve the representation of seasonal changes in numerical ice sheet models, future work should evaluate the ability of climate models to reproduce seasonal amplitude of ocean temperatures in the polar regions.

5 Conclusion

We have designed and performed experiments to investigate the effect of seasonal terminus oscillations on simulated multi-decadal mass loss for retreating glaciers, using an idealized glacier geometry representative of tidewater glaciers. When we compare annual-mean mass loss for simulations that include seasonal terminus oscillations with simulations that neglect oscillations, we find a bias that is strongly dependent on the magnitude of oscillations and the bed slope at the terminus. In simulations with 1250-m oscillations, we find that simulations that omit oscillations result in an overestimate of mass loss up to 18%. This offset decreases with decreasing terminus oscillation magnitude, down to $<2\%$ for 625-m oscillations. Thus, it is especially important to include seasonal terminus motion for simulations of tidewater glaciers with large seasonal oscillations, on the order of $\sim$1 km. These biases have very little sensitivity to sliding law, for the two sliding laws that we tested.

Our study has implications on ice-sheet modeling for decadal to centennial sea-level rise projections. Our results motivate the need for a comprehensive study on the observed seasonalities of tidewater glacier advance and retreat. An investigation into the observed relationship between the magnitude of seasonal retreat and advance, bed topography, and basal sliding would improve our understanding for how to best model these systems. There is also a need for additional modeling to go beyond idealized glaciers and simulate real glaciers, attempting to reconstruct their behavior using past observations of seasonal terminus motion.

In order to simulate seasonal variability of the ice sheets, observations and forcings that adequately capture seasonal variability are needed. Seasonal measurements of ice mass change from satellite gravimetry at spatial scales of hundreds of kilometers have been available since the early 2000s. Seasonal observations of surface velocities are available and have been used to characterize seasonal patterns of tidewater glacier acceleration and deceleration as well as to infer which glaciers are controlled by runoff (Vijay et al., 2019; Moon et al., 2014). However, high spatial resolution surface elevation change observations, such as those from satellite altimetry and photogrammetry, are needed to localize measured change from gravimetry to the scales of individual tidewater glaciers and to complement velocity observations in analysis of glacier force balance. Repeat measurements of the ice sheets, which will enable the measurement of tidewater glacier thickness change, are only now starting to become available with the recent launch of NASA's ICESat-2 mission. Terminus positions at seasonal temporal resolution are also only recently starting to become available for many tidewater glaciers around the entire ice sheet. Ice sheet projections for follow-on efforts to ISMIP6 would benefit from a consistent set of forcings and observations of tidewater glacier change at seasonal temporal resolution.

Acknowledgments

DF was supported by an appointment to the NASA Postdoctoral Program at the NASA Goddard Space Flight Center, administered by Universities Space Research Association under contract with NASA. SN was supported by grants from the NASA Sea-Level Change Team (N-SLCT), Cryospheric Science, and Modeling, Analysis and Prediction (MAP) programs. MM was supported by the Heising Simons Foundation (grant #2019-1161). Work was performed by HS at the Jet Propulsion Laboratory, California Institute of Technology, under a contract with the National Aeronautics and Space Administration; support was provided by grants from NASA Cryospheric Science and Modeling, Analysis and Prediction (MAP) programs and by JPL Research and Technology Development program. ISSM is free and open source software that can be downloaded from `https://issm.jpl.nasa.gov`. Configuration scripts to setup and run all simulations can be obtained from `https://github.com/dfelikson/TWG_idealized_glacier_response` (We will publish our code with a DOI via Zenodo once the manuscript is ready for publication).

References

Asay-Davis, X. S., Cornford, S. L., Durand, G., Galton-Fenzi, B. K., Gladstone, R. M., Gudmundsson, G. H., ... Seroussi, H. (2016). Experimental design for three interrelated marine ice sheet and ocean model intercomparison projects: MISMIP v. 3 (MISMIP +), ISOMIP v. 2 (ISOMIP +) and MISOMIP v. 1 (MISOMIP1). *Geoscientific Model Development*, *9*(7), 2471–2497.

Barthel, A., Agosta, C., Little, C. M., Hattermann, T., Jourdain, N. C., Goelzer, H., ... Bracegirdle, T. J. (2020, March). CMIP5 model selection for ISMIP6 ice sheet model forcing: Greenland and Antarctica. *The Cryosphere*, *14*, 855–879.

Bevan, S. L., Luckman, A. J., & Murray, T. (2012). Glacier dynamics over the last quarter of a century at Helheim, Kangerdlugssuaq and 14 other major Greenland outlet glaciers. *The Cryosphere*, *6*(5), 923–937.

Bondzio, J. H., Morlighem, M., Seroussi, H., Kleiner, T., Rückamp, M., Mouginot, J., ... Humbert, A. (2017, June). The mechanisms behind Jakobshavn Isbrae's acceleration and mass loss: A 3-D thermomechanical model study. *Geophysical Research Letters*, *322*(5906), 1344.

Bondzio, J. H., Seroussi, H., Morlighem, M., Kleiner, T., Rückamp, M., Humbert, A., & Larour, E. Y. (2016). Modelling calving front dynamics using a level-set method: application to Jakobshavn Isbræ, West Greenland. *The Cryosphere*, *10*(2), 497–510.

Brondex, J., Gagliardini, O., Gillet-Chaulet, F., & Durand, G. (2017, October). Sensitivity of grounding line dynamics to the choice of the friction law. *Journal of Glaciology*, *63*(241), 854–866.

Brondex, J., Gillet-Chaulet, F., & Gagliardini, O. (2019). Sensitivity of centennial mass loss projections of the Amundsen basin to the friction law. *The Cryosphere*, *13*(1), 177–195.

Budd, W. F., Keage, P. L., & Blundy, N. A. (1979). Empirical studies of ice sliding. *Journal of Glaciology*, *23*(89), 157–170.

Bulthuis, K., Arnst, M., Sun, S., & Pattyn, F. (2019). Uncertainty quantification of the multi-centennial response of the Antarctic ice sheet to climate change. *The Cryosphere*, *13*(4), 1349–1380.

Catania, G. A., Stearns, L. A., Sutherland, D. A., Fried, M. J., Bartholomaus, T. C., Morlighem, M., ... Nash, J. (2018, August). Geometric Controls on Tidewater Glacier Retreat in Central Western Greenland. *Journal of Geophysical Research: Earth Surface*, *29*(1), 1–15.

Cheng, D., Hayes, W., Larour, E., Mohajerani, Y., Wood, M., Velicogna, I., & Rignot, E. (2021). Calving Front Machine (CALFIN): Glacial Termini Dataset and Automated Deep Learning Extraction Method for Greenland, 1972-2019.

The Cryosphere, *15*, 16631675.
Choi, Y., Morlighem, M., Rignot, E., & Wood, M. (2021, January). Ice dynamics will remain a primary driver of Greenland ice sheet mass loss over the next century. *Communications Earth & Environment*, 1–9.
Cornford, S. L., Seroussi, H., Asay-Davis, X. S., Gudmundsson, G. H., Arthern, R., Borstad, C., … Yu, H. (2020). Results of the third Marine Ice Sheet Model Intercomparison Project (MISMIP+). *The Cryosphere*, *14*, 2283–2301.
Csatho, B. M., Schenk, A. F., van der Veen, C. J., Babonis, G., Duncan, K., Rezvanbehbahani, S., … van Angelen, J. H. (2014, December). Laser altimetry reveals complex pattern of Greenland Ice Sheet dynamics. *Proceedings of the National Academy of Sciences*, *111*(52), 18478–18483.
Davison, B. J., Sole, A. J., Cowton, T. R., Lea, J. M., Slater, D. A., Fahrner, D., & Nienow, P. W. (2020, September). Subglacial Drainage Evolution Modulates Seasonal Ice Flow Variability of Three Tidewater Glaciers in Southwest Greenland. *Journal of Geophysical Research: Earth Surface*, *125*(9), e2019JF005492.
Edwards, T. L., Brandon, M. A., Durand, G., Edwards, N. R., Golledge, N. R., Holden, P. B., … Wernecke, A. (2019, January). Revisiting Antarctic ice loss due to marine ice-cliff instability. *Nature*, *566*(7742), 58–64.
Fahrner, D., Lea, J. M., Brough, S., Mair, D. W. F., & Abermann, J. (2021, February). Linear response of the Greenland ice sheet's tidewater glacier terminus positions to climate. *Journal of Glaciology*, 1–11.
Felikson, D., Urban, T. J., Gunter, B. C., Pie, N., Pritchard, H. D., Harpold, R., & Schutz, B. E. (2017, October). Comparison of Elevation Change Detection Methods From ICESat Altimetry Over the Greenland Ice Sheet. *IEEE Transactions on Geoscience and Remote Sensing*, *55*(10), 5494–5505.
Fried, M. J., Catania, G. A., Stearns, L. A., Sutherland, D. A., Bartholomaus, T. C., Shroyer, E., & Nash, J. (2018, July). Reconciling Drivers of Seasonal Terminus Advance and Retreat at 13 Central West Greenland Tidewater Glaciers. *Journal of Geophysical Research: Earth Surface*, *115*(73), F01005–18.
Gagliardini, O., Cohen, D., Råback, P., & Zwinger, T. (2007, June). Finite-element modeling of subglacial cavities and related friction law. *Journal of Geophysical Research: Earth Surface*, *112*(F2), F02027.
Gardner, A. S., Fahnestock, M. A., & Scambos, T. A. (2019). *ITS_LIVE Regional Glacier and Ice Sheet Surface Velocities.* Retrieved from `http://dx.doi.org/10.5067/6II6VW8LLWJ7` (NASA National Snow and Ice Data Center Distributed Active Archive Center) doi: 10.5067/6II6VW8LLWJ7
Gardner, A. S., Moholdt, G., Cogley, J. G., Wouters, B., Arendt, A. A., Wahr, J., … Paul, F. (2013, May). A Reconciled Estimate of Glacier Contributions to Sea Level Rise: 2003 to 2009. *Science*, *340*(6134), 852–857.
Gardner, A. S., Moholdt, G., Scambos, T. A., Fahnstock, M., Ligtenberg, S., van den Broeke, M. R., & Nilsson, J. (2018). Increased West Antarctic and unchanged East Antarctic ice discharge over the last 7 years. *The Cryosphere*, *12*(2), 521–547.
Goelzer, H., Nowicki, S., Payne, A., Larour, E., Seroussi, H., Lipscomb, W. H., … Broeke, M. v. d. (2020, January). The future sea-level contribution of the Greenland ice sheet: a multi-model ensemble study of ISMIP6. *The Cryosphere Discussions*.
Hecht, F. (2006, May). *BAMG: Bidimensional Anisotropic Mesh Generator* (Tech. Rep.).
Hoffman, M. J., Asay-Davis, X., Price, S. F., Fyke, J., & Perego, M. (2019). Effect of Subshelf Melt Variability on Sea Level Rise Contribution From Thwaites Glacier, Antarctica. *Journal of Geophysical Research: Earth Surface*, *124*, 2798–2822.
Howat, I. M., Smith, B. E., Joughin, I. R., & Scambos, T. A. (2008, September).

Rates of southeast Greenland ice volume loss from combined ICESat and ASTER observations. *Geophysical Research Letters*, *35*(17), L17505.
Jacob, T., Wahr, J., Pfeffer, W. T., & SWENSON, S. (2012, February). Recent contributions of glaciers and ice caps to sea level rise. *Nature*, 1–5.
Larour, E. Y., Seroussi, H., Morlighem, M., & Rignot, E. (2012, March). Continental scale, high order, high spatial resolution, ice sheet modeling using the Ice Sheet System Model (ISSM). *Journal of Geophysical Research*, *117*(F1).
Luthcke, S. B., Sabaka, T. J., Loomis, B. D., Arendt, A. A., McCarthy, J. J., & camp, J. (2013, August). Antarctica, Greenland and Gulf of Alaska land-ice evolution from an iterated GRACE global mascon solution. *Journal of Glaciology*, *59*(216), 613–631.
MacAyeal, D. R. (1989, April). Large-scale ice flow over a viscous basal sediment: theory and application to Ice Stream B, Antarctica. *Journal of Geophysical Research*, *94*(B4), 4071–4087.
Mantelli, E., Bertagni, M. B., & Ridolfi, L. (2016, November). Stochastic ice stream dynamics. *Proceedings of the National Academy of Sciences*, *113*(47), E4594–E4600.
Moon, T., Joughin, I. R., & Smith, B. E. (2015, May). Seasonal to multiyear variability of glacier surface velocity, terminus position, and sea ice/ice mélange in northwest Greenland. *Journal of Geophysical Research: Earth Surface*, *120*(5), 818–833.
Moon, T., Joughin, I. R., Smith, B. E., van den Broeke, M. R., van de Berg, W. J., Noël, B. P. Y., & Usher, M. (2014, October). Distinct patterns of seasonal Greenland glacier velocity. *Geophysical Research Letters*, *41*(20), 7209–7216.
Mouginot, J., Rignot, E., Bjørk, A. A., van den Broeke, M. R., Millan, R., Morlighem, M., … Wood, M. (2019, April). Forty-six years of Greenland Ice Sheet mass balance from 1972 to 2018. *Proceedings of the National Academy of Sciences*, *116*(19), 9329–9244.
Muresan, I. S., Khan, S. A., Aschwanden, A., Khroulev, C., van Dam, T. M., Bamber, J. L., … Kjær, K. H. (2016). Modelled glacier dynamics over the last quarter of a century at Jakobshavn Isbræ. *The Cryosphere*, *10*(2), 597–611.
Murray, T., Scharrer, K., Selmes, N., Booth, A. D., James, T. D., Bevan, S. L., … McGovern, J. (2015, August). Extensive Retreat of Greenland Tidewater Glaciers, 2000–2010. *Arctic, Antarctic, and Alpine Research*, *47*(3), 427–447.
Nias, I. J., Cornford, S. L., Edwards, T. L., Gourmelen, N., & Payne, A. J. (2019, October). Assessing Uncertainty in the Dynamical Ice Response to Ocean Warming in the Amundsen Sea Embayment, West Antarctica. *Geophysical Research Letters*, *46*(20), 11253–11260.
Nias, I. J., Cornford, S. L., & Payne, A. J. (2016). Contrasting the modelled sensitivity of the Amundsen Sea Embayment ice streams. *Journal of Glaciology*, *62*(233), 552–562.
Nowicki, S., Payne, A. J., Goelzer, H., Seroussi, H., Lipscomb, W. H., Abe-Ouchi, A., … van de Wal, R. (2020, January). Experimental protocol for sea level projections from ISMIP6 standalone ice sheet models . *The Cryosphere Discussions*.
Phillips, T., Rajaram, H., & Steffen, K. (2010, October). Cryo-hydrologic warming: A potential mechanism for rapid thermal response of ice sheets. *Geophysical Research Letters*, *37*(20), L20503.
Rignot, E., Mouginot, J., Scheuchl, B., van den Broeke, M. R., van Wessem, M. J., & Morlighem, M. (2019, January). Four decades of Antarctic Ice Sheet mass balance from 1979–2017. *Proceedings of the National Academy of Sciences*, *116*(4), 1095–1103.
Ritz, C., Durand, G., Payne, A. J., Peyaud, V., Hindmarsh, R. C. A., & Edwards, T. L. (2015, November). Potential sea-level rise from Antarctic ice-sheet instability constrained by observations. *Nature*, *528*, 115–118.

Robel, A. A., Roe, G. H., & Haseloff, M. (2018, September). Response of Marine-Terminating Glaciers to Forcing: Time Scales, Sensitivities, Instabilities, and Stochastic Dynamics. *Journal of Geophysical Research: Earth Surface*, *62*(231), 82–23.

Robel, A. A., Seroussi, H., & Roe, G. H. (2019, July). Marine ice sheet instability amplifies and skews uncertainty in projections of future sea-level rise. *Proceedings of the National Academy of Sciences*, *116*(30), 14887–14892.

Ruckert, K. L., Shaffer, G., Pollard, D., Guan, Y., Wong, T. E., Forest, C. E., & Keller, K. (2017, January). Assessing the Impact of Retreat Mechanisms in a Simple Antarctic Ice Sheet Model Using Bayesian Calibration. *PLOS ONE*, *12*(1), e0170052–15.

Schild, K. M., & Hamilton, G. S. (2013). Seasonal variations of outlet glacier terminus position in Greenland. *Journal of Glaciology*, *59*(216), 759–770.

Schoof, C. (2005, March). The effect of cavitation on glacier sliding. *Proceedings of the Royal Society A: Mathematical, Physical and Engineering Sciences*, *461*(2055), 609–627.

Schrama, E. J. O., & Wouters, B. (2011, February). Revisiting Greenland ice sheet mass loss observed by GRACE. *Journal of Geophysical Research*, *116*(B2), B02407.

Seroussi, H., & Morlighem, M. (2018). Representation of basal melting at the grounding line in ice flow models. *The Cryosphere*, *12*(10), 3085–3096.

Seroussi, H., Nowicki, S., Payne, A. J., Goelzer, H., Lipscomb, W. H., Abe-Ouchi, A., … Zwinger, T. (2020, January). ISMIP6 Antarctica: a multi-model ensemble of the Antarctic ice sheet evolution over the 21st century. *The Cryosphere Discussions*.

Shepherd, A. P., Ivins, E., Rignot, E., Smith, B. E., van den Broeke, M. R., Velicogna, I., … Wuite, J. (2020, February). Mass balance of the Greenland Ice Sheet from 1992 to 2018. *Nature*, 1–21.

Smith, L. C., Andrews, L. C., Pitcher, L. H., Overstreet, B. T., Rennermalm, Å. K., Cooper, M. G., … Simpson, C. E. (2021, April). Supraglacial River Forcing of Subglacial Water Storage and Diurnal Ice Sheet Motion. *Geophysical Research Letters*, *48*(7), e2020GL091418.

Sun, S., Pattyn, F., Simon, E. G., Albrecht, T., Cornford, S., Calov, R., … Zhang, T. (2020, September). Antarctic ice sheet response to sudden and sustained ice-shelf collapse (ABUMIP). *Journal of Glaciology*, *66*(260), 891–904.

The IMBIE team. (2018, June). Mass balance of the Antarctic Ice Sheet from 1992 to 2017. *Nature*, *558*(7709), 219–222.

Tsai, V. C., Stewart, A. L., & Thompson, A. F. (2015, July). Marine ice-sheet profiles and stability under Coulomb basal conditions. , 1–11.

Velicogna, I., Mohajerani, Y., Geruo, A., Landerer, F. W., Mouginot, J., Noël, B. P. Y., … Wiese, D. (2020, March). Continuity of ice sheet mass loss in Greenland and Antarctica from the GRACE and GRACE Follow-Onmissions. *Geophysical Research Letters*, e2020GL087291–16.

Velicogna, I., & Wahr, J. (2013, June). Time-variable gravity observations of ice sheet mass balance: Precision and limitations of the GRACE satellite data. *Geophysical Research Letters*, *40*(12), 3055–3063.

Vijay, S., Khan, S. A., Kusk, A., Solgaard, A. M., Moon, T., & Bjørk, A. A. (2019, February). Resolving Seasonal Ice Velocity of 45 Greenlandic Glaciers With Very High Temporal Details. *Geophysical Research Letters*, *46*(3), 1485–1495.

Weertman, J. (1957, March). On the sliding of glaciers. *Journal of Glaciology*, *3*, 33–38.

Zhang, E., Liu, L., & Huang, L. (2019, June). Automatically delineating the calving front of Jakobshavn Isbræ from multitemporal TerraSAR-X images: a deep learning approach. *The Cryosphere*, *13*, 1729–1741.

JOURNAL OF GEOPHYSICAL RESEARCH

Supporting Information for "Seasonal tidewater glacier terminus oscillations bias multi-decadal projections of ice mass change"

D. Felikson[1,2] *, S. Nowicki[3], I. Nias[4], M. Morlighem[5], H. Seroussi[6]

[1]Cryospheric Sciences Laboratory, NASA Goddard Space Flight Center, Greenbelt, MD, USA

[2]Goddard Earth Sciences Technology and Research Studies and Investigations, Universities Space Research Association, Columbia, MD, USA

[3]Department of Geology, University at Buffalo, Buffalo, NY, USA

[4]School of Environmental Sciences, University of Liverpool, Liverpool, UK

[5]Department of Earth System Science, University of California, Irvine, Irvine, CA, USA

[6]Jet Propulsion Laboratory, California Institute of Technology, Pasadena, CA, USA

Contents of this file

Additional Supporting Information (Files uploaded separately)

1. Captions for Movies S1 to S12

Corresponding author: D. Felikson, Cryospheric Sciences Laboratory, NASA Goddard Space Flight Center, Greenbelt, MD, USA (denis.felikson@nasa.gov)

*Address

Introduction

The supporting information includes 1 figure and 12 movies. The figure (Fig. S1) presents the same data as Fig. 4 in the main text, with two additional simulations for each set of model parameters: a simulation in which the terminus remains fixed at the initial position (triangles pointing up in Fig. S1) and a simulation in which the terminus retreats to the most retreated seasonal position (triangles pointing down in Fig. S1). These additional results bound the simulations in which the terminus oscillates (lines without x's in Fig. S1) and those in which the terminus retreats to the mean seasonal position (line with x's in Fig. S1) and are discussed in the main text. The movies (Movies S1 to S12) show thickness change and velocity change in map view for the simulations with Budd sliding, terminus on retrograde bed slope, with and without seasonal oscillations.

Movie S1. Thickness change, with respect to initial thickness, for simulation with Budd sliding, terminus on retrograde bed slope, and 625-m seasonal terminus oscillations. Red line represents the location of the terminus.

Movie S2. Velocity change, with respect to initial velocity, for simulation with Budd sliding, terminus on retrograde bed slope, and 625-m seasonal terminus oscillations. Red line represents the location of the terminus.

Movie S3. Thickness change, with respect to initial thickness, for simulation with Budd sliding, terminus on retrograde bed slope, and terminus retreat of 312.5 m (mean of 625-m oscillations). Red line represents the location of the terminus.

Movie S4. Velocity change, with respect to initial velocity, for simulation with Budd sliding, terminus on retrograde bed slope, and retreat of 312.5 m (mean of 625-m oscillations). Red line represents the location of the terminus.

Movie S5. Thickness change, with respect to initial thickness, for simulation with Budd sliding, terminus on retrograde bed slope, and 937.5-m seasonal terminus oscillations. Red line represents the location of the terminus.

Movie S6. Velocity change, with respect to initial velocity, for simulation with Budd sliding, terminus on retrograde bed slope, and 625-m seasonal terminus oscillations. Red line represents the location of the terminus.

Movie S7. Thickness change, with respect to initial thickness, for simulation with Budd sliding, terminus on retrograde bed slope, and terminus retreat of 468.75 m (mean of 937.5-m oscillations). Red line represents the location of the terminus.

Movie S8. Velocity change, with respect to initial velocity, for simulation with Budd sliding, terminus on retrograde bed slope, and retreat of 468.75 m (mean of 937.5-m oscillations). Red line represents the location of the terminus.

Movie S9. Thickness change, with respect to initial thickness, for simulation with Budd sliding, terminus on retrograde bed slope, and 1250-m seasonal terminus oscillations. Red line represents the location of the terminus.

Movie S10. Velocity change, with respect to initial velocity, for simulation with Budd sliding, terminus on retrograde bed slope, and 625-m seasonal terminus oscillations. Red line represents the location of the terminus.

Movie S11. Thickness change, with respect to initial thickness, for simulation with Budd sliding, terminus on retrograde bed slope, and terminus retreat of 625 m (mean of 1250-m oscillations). Red line represents the location of the terminus.

Movie S12. Velocity change, with respect to initial velocity, for simulation with Budd sliding, terminus on retrograde bed slope, and retreat of 625 m (mean of 1250-m oscillations). Red line represents the location of the terminus.

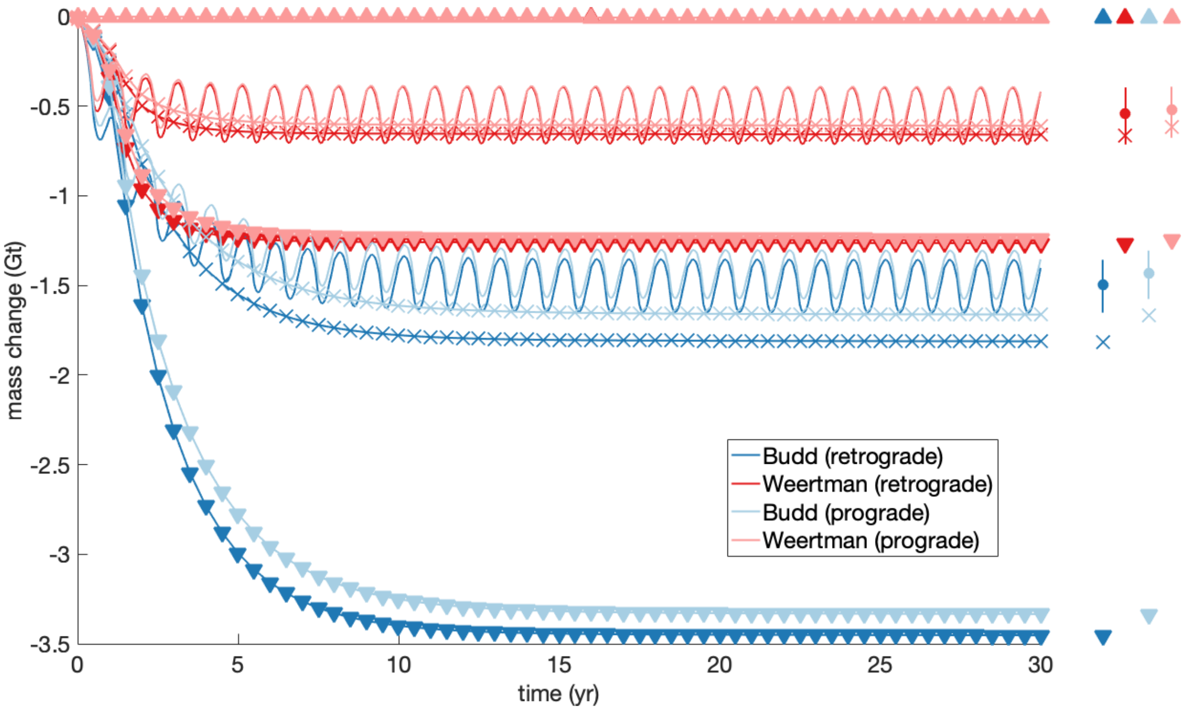

Figure S1. Glacier mass change for Budd (blue) and Weertman (red) sliding laws on prograde (lighter lines) and retrograde (darker lines) bed slope. Change in mass above floatation shown for four simulations: (1) no seasonality (line with x's), (2) with seasonality (no x's), (3) no motion (line with triangles pointing up), and (4) terminus at most retreated position (line with triangles pointing down). To the right of the time series, filled circles represent mean mass change and vertical lines represent seasonal amplitude of mass change during final year of simulation.